Supporting Information for "Different types of corona discharges associated with high-altitude positive Narrow Bipolar Events nearby cloud top"

Dongshuai Li[1,2], Alejandro Luque[1], F. J. Gordillo-Vazquez[1],

F. J. Pérez-Invernón[1], Lasse Skaaning Husbjerg[2], Torsten Neubert[2],

Olivier Chanrion[2], Gaopeng Lu[3], Hongbo Zhang[4], Jing Han[5],

Nikolai G. Lehtinen[6], Nikolai Østgaard[6], Víctor Reglero[7]

[1]Instituto de Astrofísica de Andalucía (IAA), CSIC, Granada, Spain.

[2]National Space Institute, Technical University of Denmark (DTU Space), Kongens Lyngby, Denmark.

[3]CAS Key Laboratory of Geospace Environment,

University of Science and Technology of China, Hefei, China.

[4]Key Laboratory of Middle Atmosphere and Global Environment Observation (LAGEO),

Institute of Atmospheric Science, Chinese Academy of Sciences, Beijing, China.

[5]Hainan Institute of Meteorological Sciences, Haikou, China

[6]Birkeland Centre for Space Science, Department of Physics and Technology,

University of Bergen, Bergen, Norway

[7]Image Processing Laboratory, University of Valencia, Valencia, Spain

Contents of this file

1. Figure S1: The time shift for MMIA with respect to the ground-based radio signals for the corona discharges.

2. Figure S2 - S22: Comparison between Modular Multispectral Imaging Array (MMIA) observation and the modeling result of the first-hitting-time model along with the magnetic field components B_ϕ detected from the ground-based very low frequency/low frequency (VLF/LF) sensor at Malaysia for the corona discharges.

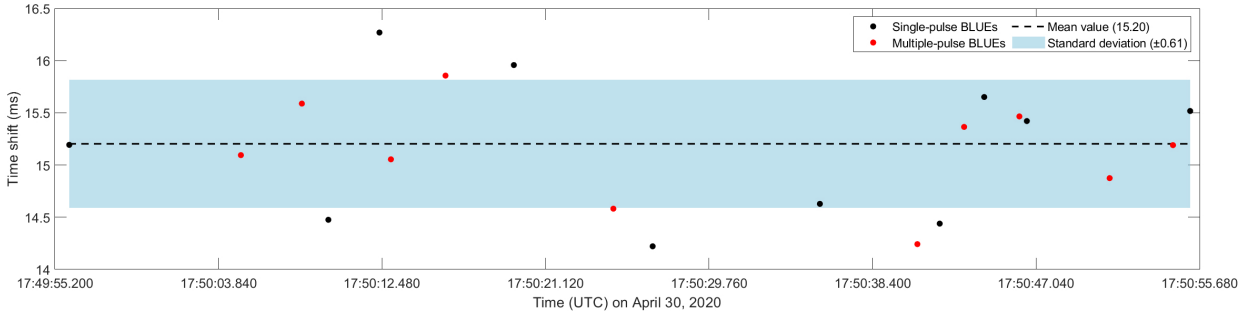

Figure S1. The time shift of MMIA with respect to the ground-based VLF/LF radio signals for 21 corona discharges (10 single-pulse BLUEs (black dots) and 11 multiple-pulse BLUEs (red dots)). The mean value of the MMIA time shift is about 15 ms with the standard deviation ±0.6 ms.

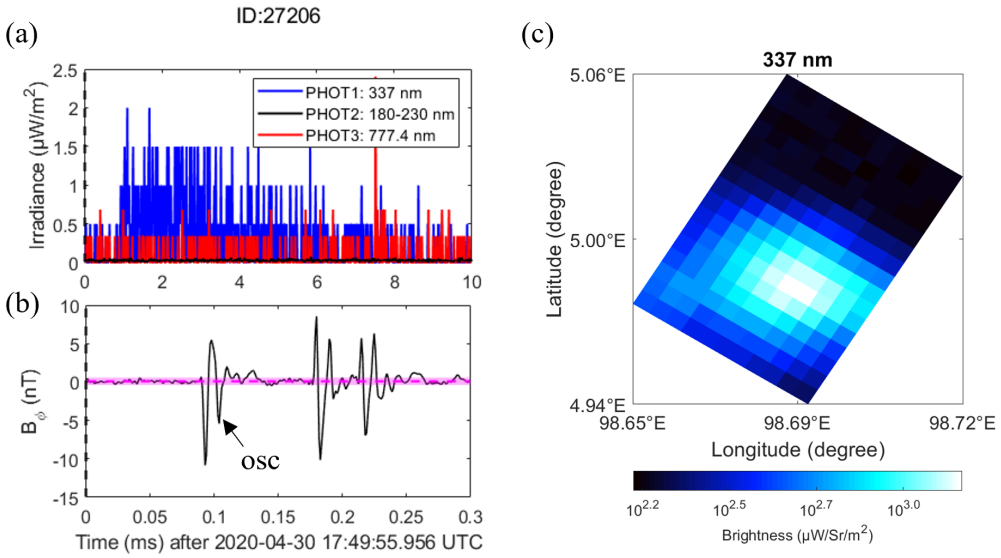

Figure S2. Comparison between MMIA photometer irradiance (blue: 337 nm, black: 180-230 nm and red: 777.4 nm) (a) and its corresponding NBE pulse (b) detected from the ground-based VLF/LF sensor nearby Malaysia for the single-pulse BLUE with ID 27206. The corresponding 337-nm filtered image of MMIA is shown in (c). The pink horizontal dashed line is the mean of the background noises with the pink shaded band $\mu \pm 3\sigma$. The oscillations are marked as *OSC* in the figure.

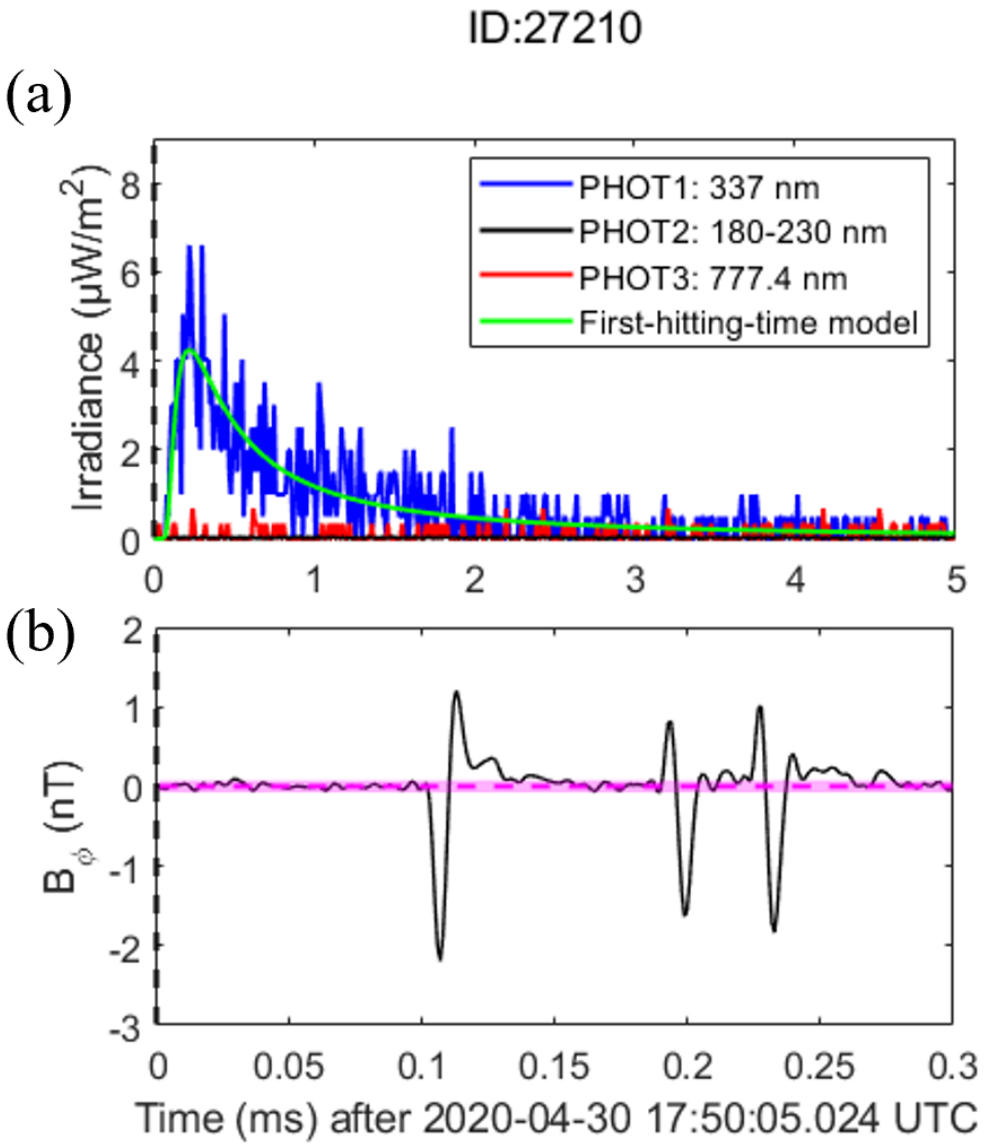

Figure S3. Comparison between MMIA photometer irradiance (blue: 337 nm, black: 180-230 nm, red: 777.4 nm and green: modeling result of the first-hitting-time model) (a) and its corresponding NBE pulse (b) detected from the ground-based VLF/LF sensor nearby Malaysia for the single-pulse BLUE with ID 27210. There is no corresponding 337-nm filtered image detected by MMIA. The pink horizontal dashed line is the mean of the background noises with the pink shaded band $\mu \pm 3\sigma$.

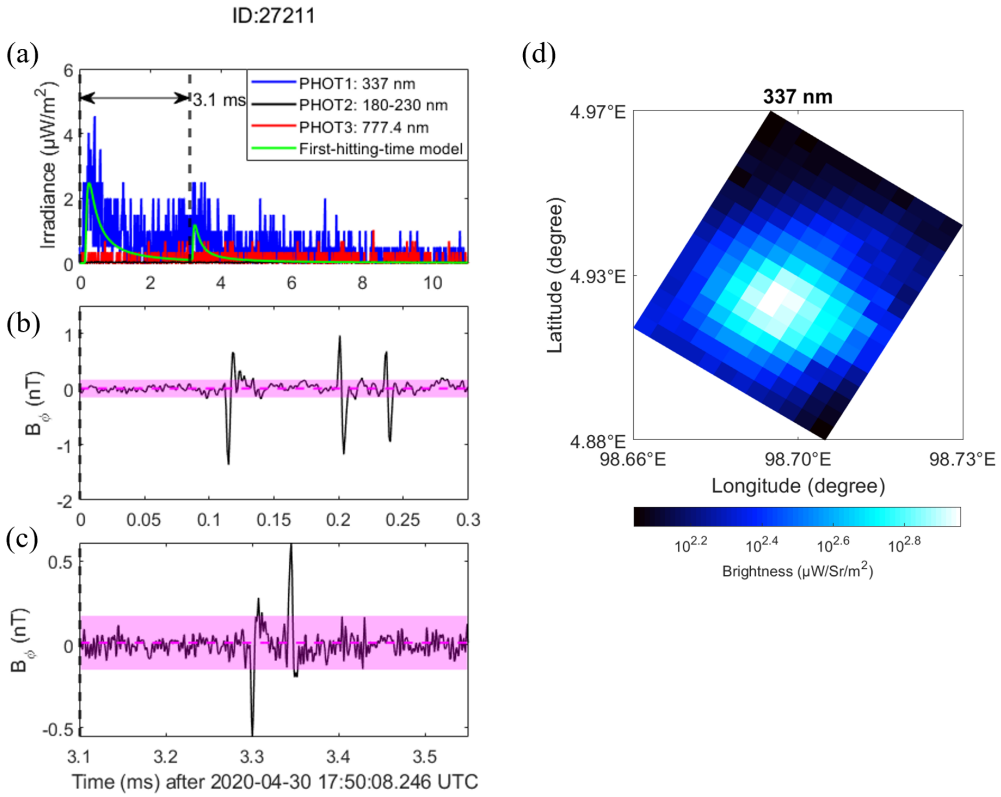

Figure S4. Comparison between MMIA photometer irradiance (blue: 337 nm, black: 180-230 nm, red: 777.4 nm and green: modeling result of the first-hitting-time model) (a) and its corresponding NBE pulse (b) and the subsequent pulses trains (c) detected from the ground-based VLF/LF sensor nearby Malaysia for the multiple-pulse BLUE with ID 27211. The corresponding 337-nm filtered image of MMIA is shown in (d). The pink horizontal dashed line is the mean of the background noises with the pink shaded band $\mu \pm 3\sigma$.

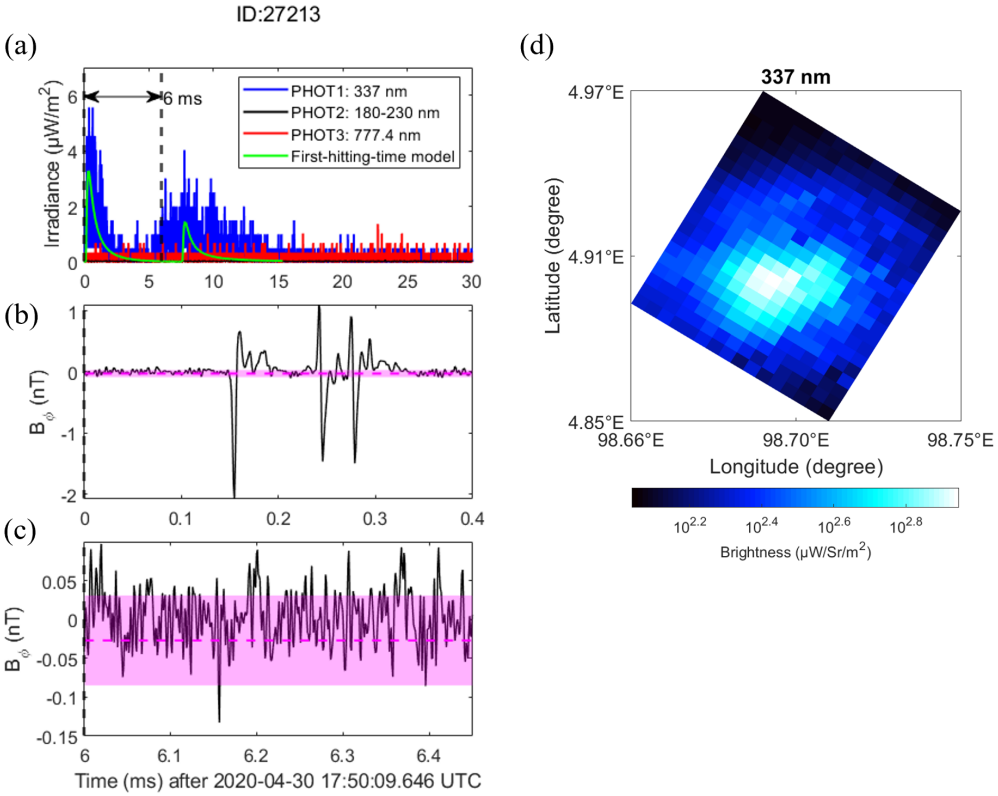

Figure S5. Comparison between MMIA photometer irradiance (blue: 337 nm, black: 180-230 nm, red: 777.4 nm and green: modeling result of the first-hitting-time model) (a) and its corresponding NBE pulse (b) and the subsequent pulses trains (c) detected from the ground-based VLF/LF sensor nearby Malaysia for the multiple-pulse BLUE with ID 27213. The corresponding 337-nm filtered image of MMIA is shown in (d). The pink horizontal dashed line is the mean of the background noises with the pink shaded band $\mu \pm 3\sigma$.

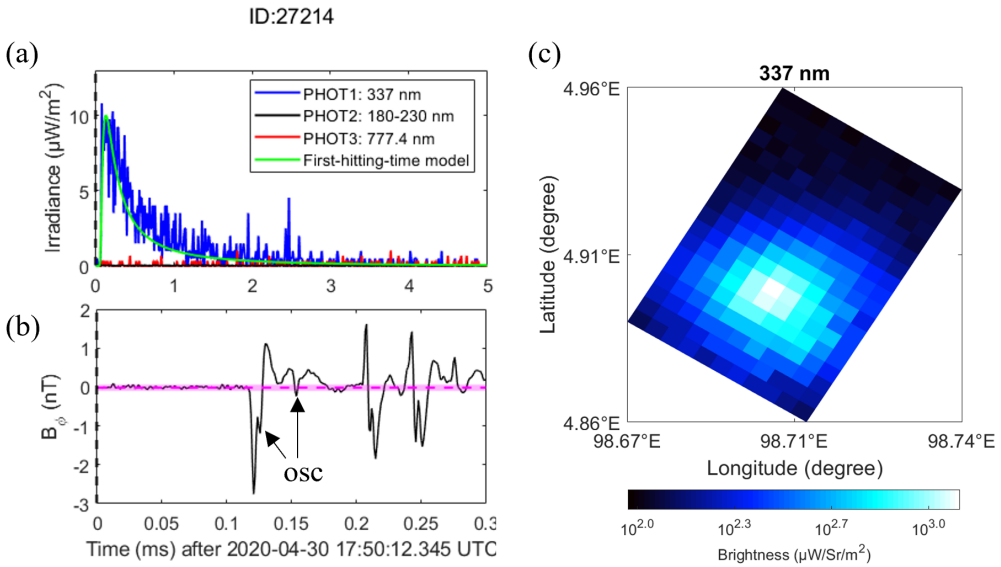

Figure S6. Comparison between MMIA photometer irradiance (blue: 337 nm, black: 180-230 nm, red: 777.4 nm and green: modeling result of the first-hitting-time model) (a) and its corresponding NBE pulse (b) detected from the ground-based VLF/LF sensor nearby Malaysia for the single-pulse BLUE with ID 27214. The corresponding 337-nm filtered image of MMIA is shown in (c). The pink horizontal dashed line is the mean of the background noises with the pink shaded band $\mu \pm 3\sigma$. The oscillations are marked as *OSC* in the figure.

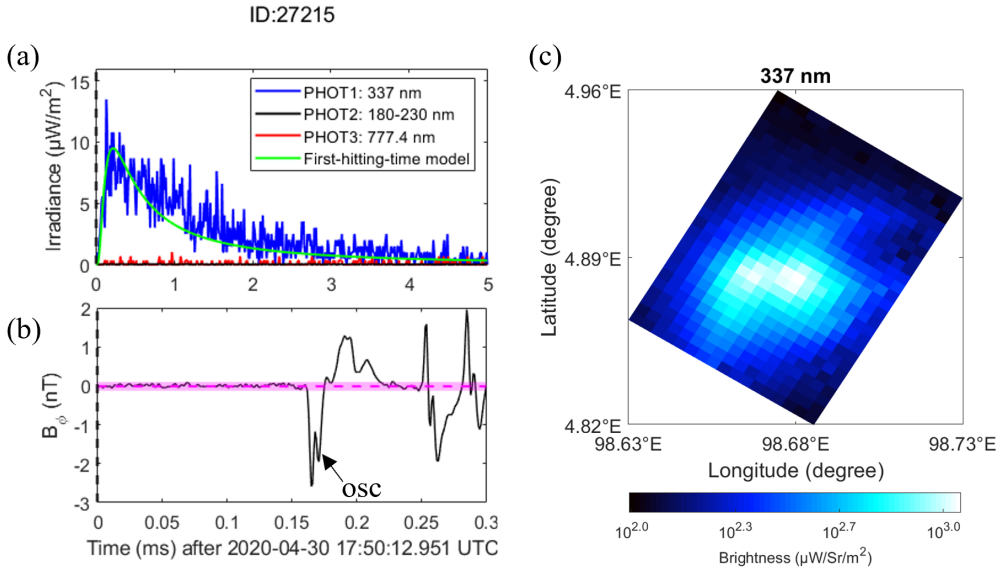

Figure S7. Comparison between MMIA photometer irradiance (blue: 337 nm, black: 180-230 nm, red: 777.4 nm and green: modeling result of the first-hitting-time model) (a) and its corresponding NBE pulse (b) detected from the ground-based VLF/LF sensor nearby Malaysia for the single-pulse BLUE with ID 27215. The corresponding 337-nm filtered image of MMIA is shown in (c). The pink horizontal dashed line is the mean of the background noises with the pink shaded band $\mu \pm 3\sigma$. The oscillations are marked as *OSC* in the figure.

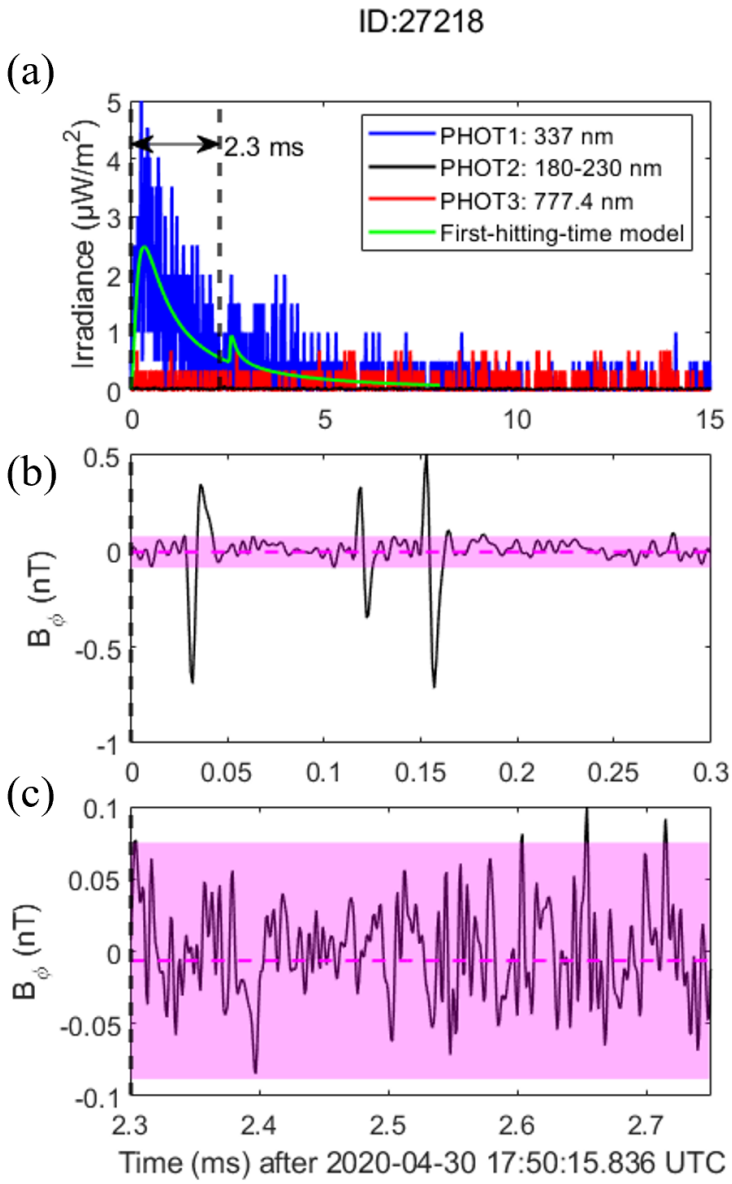

Figure S8. Comparison between MMIA photometer irradiance (blue: 337 nm, black: 180-230 nm, red: 777.4 nm and green: modeling result of the first-hitting-time model) (a) and its corresponding NBE pulse (b) and the subsequent pulses trains (c) detected from the ground-based VLF/LF sensor nearby Malaysia for the multiple-pulse BLUE with ID 27218. There is no corresponding 337-nm filtered image detected by MMIA. The pink horizontal dashed line is the mean of the background noises with the pink shaded band $\mu \pm 3\sigma$.

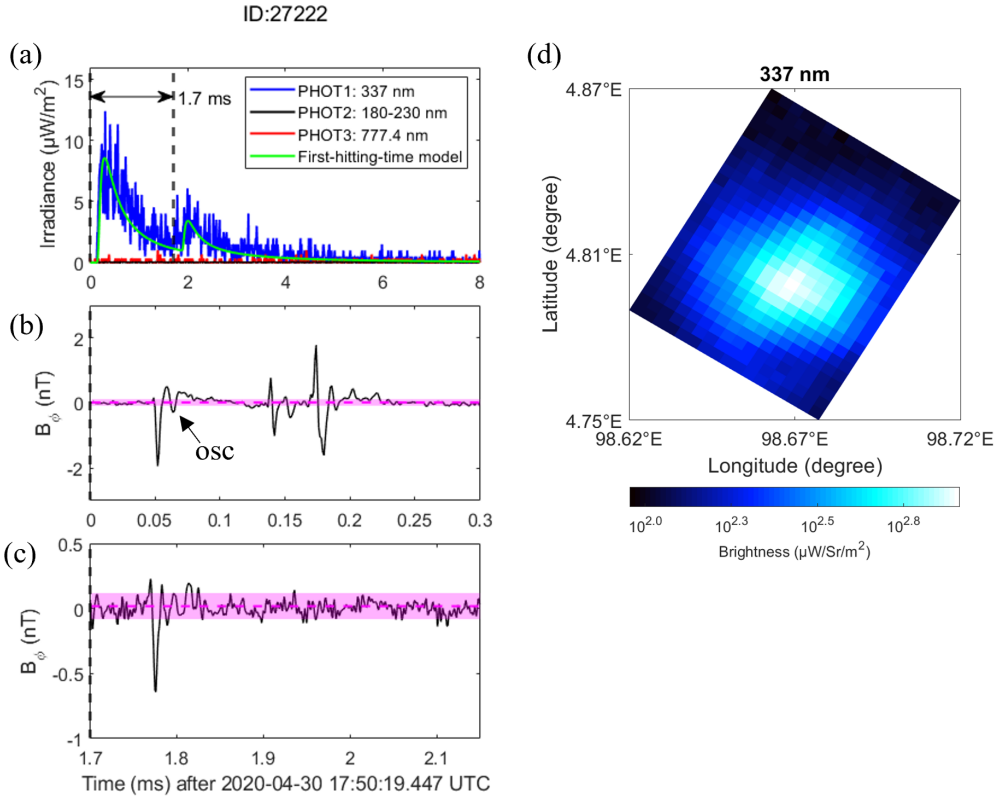

Figure S9. Comparison between MMIA photometer irradiance (blue: 337 nm, black: 180-230 nm, red: 777.4 nm and green: modeling result of the first-hitting-time model) (a) and its corresponding NBE pulse (b) and the subsequent pulses trains (c) detected from the ground-based VLF/LF sensor nearby Malaysia for the multiple-pulse BLUE with ID 27222. The corresponding 337-nm filtered image of MMIA is shown in (d). The pink horizontal dashed line is the mean of the background noises with the pink shaded band $\mu \pm 3\sigma$. The oscillations are marked as *OSC* in the figure.

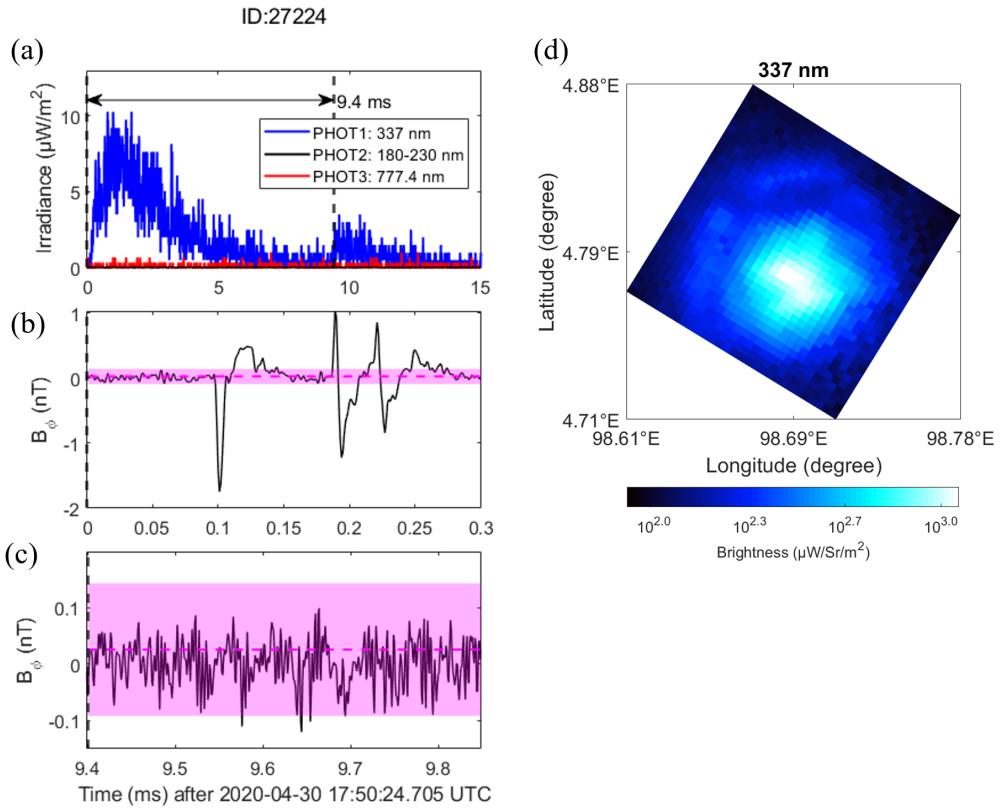

Figure S10. Comparison between MMIA photometer irradiance (blue: 337 nm, black: 180-230 nm and red: 777.4 nm) (a) and its corresponding NBE pulse (b) and the subsequent pulses trains (c) detected from the ground-based VLF/LF sensor nearby Malaysia for the multiple-pulse BLUE with ID 27224. The corresponding 337-nm filtered image of MMIA is shown in (d). The pink horizontal dashed line is the mean of the background noises with the pink shaded band $\mu \pm 3\sigma$.

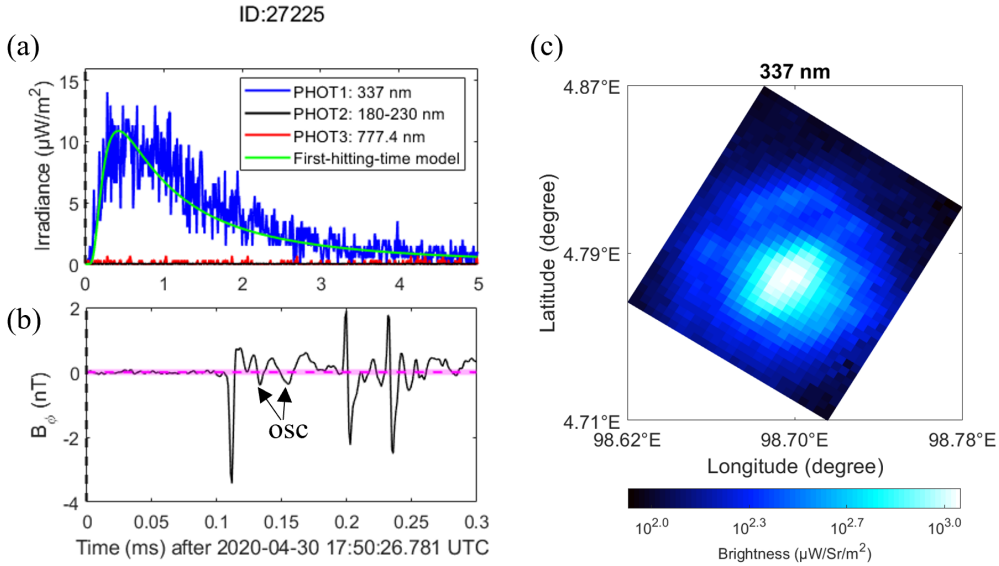

Figure S11. Comparison between MMIA photometer irradiance (blue: 337 nm, black: 180-230 nm, red: 777.4 nm and green: modeling result of the first-hitting-time model) (a) and its corresponding NBE pulse (b) detected from the ground-based VLF/LF sensor nearby Malaysia for the single-pulse BLUE with ID 27225. The corresponding 337-nm filtered image of MMIA is shown in (c). The pink horizontal dashed line is the mean of the background noises with the pink shaded band $\mu \pm 3\sigma$. The oscillations are marked as *OSC* in the figure.

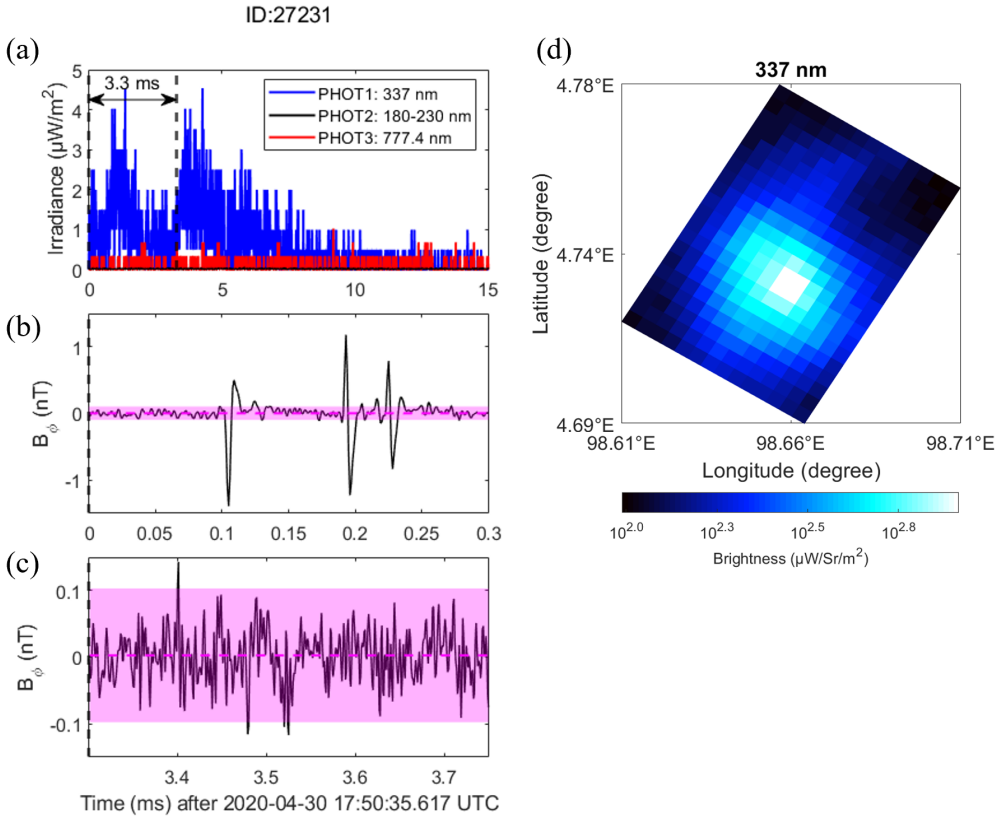

Figure S12. Comparison between MMIA photometer irradiance (blue: 337 nm, black: 180-230 nm and red: 777.4 nm) (a) and its corresponding NBE pulse (b) and the subsequent pulses trains (c) detected from the ground-based VLF/LF sensor nearby Malaysia for the multiple-pulse BLUE with ID 27231. The corresponding 337-nm filtered image of MMIA is shown in (d). The pink horizontal dashed line is the mean of the background noises with the pink shaded band $\mu \pm 3\sigma$.

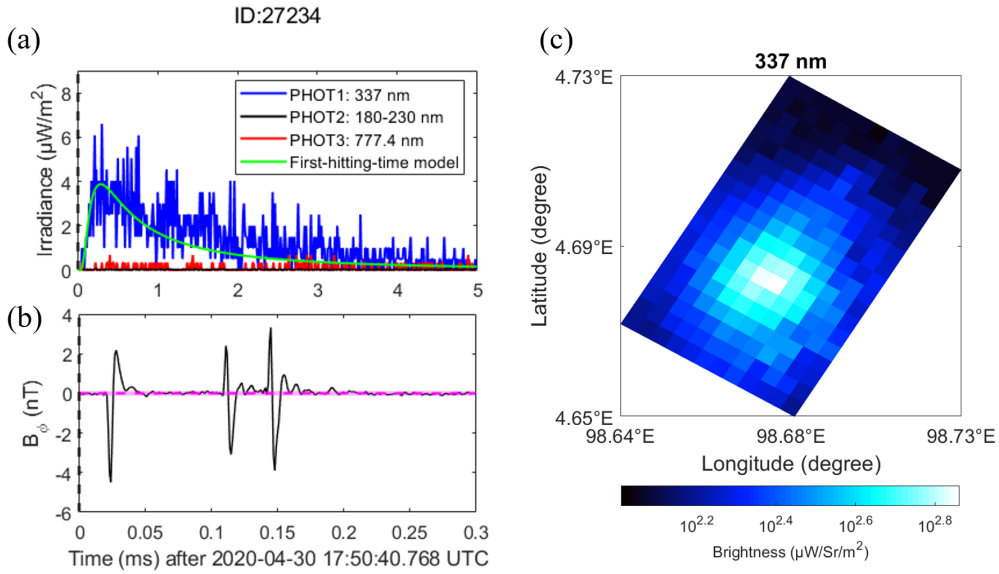

Figure S13. Comparison between MMIA photometer irradiance (blue: 337 nm, black: 180-230 nm, red: 777.4 nm and green: modeling result of the first-hitting-time model) (a) and its corresponding NBE pulse (b) detected from the ground-based VLF/LF sensor nearby Malaysia for the single-pulse BLUE with ID 27234. The corresponding 337-nm filtered image of MMIA is shown in (c). The pink horizontal dashed line is the mean of the background noises with the pink shaded band $\mu \pm 3\sigma$.

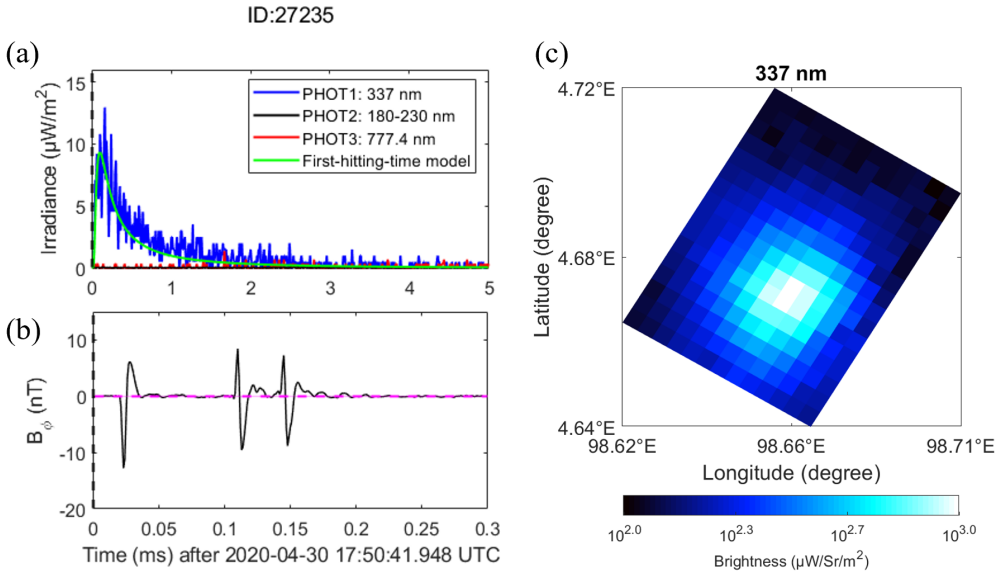

Figure S14. Comparison between MMIA photometer irradiance (blue: 337 nm, black: 180-230 nm, red: 777.4 nm and green: modeling result of the first-hitting-time model) (a) and its corresponding NBE pulse (b) detected from the ground-based VLF/LF sensor nearby Malaysia for the single-pulse BLUE with ID 27235. The corresponding 337-nm filtered image of MMIA is shown in (c). The pink horizontal dashed line is the mean of the background noises with the pink shaded band $\mu \pm 3\sigma$.

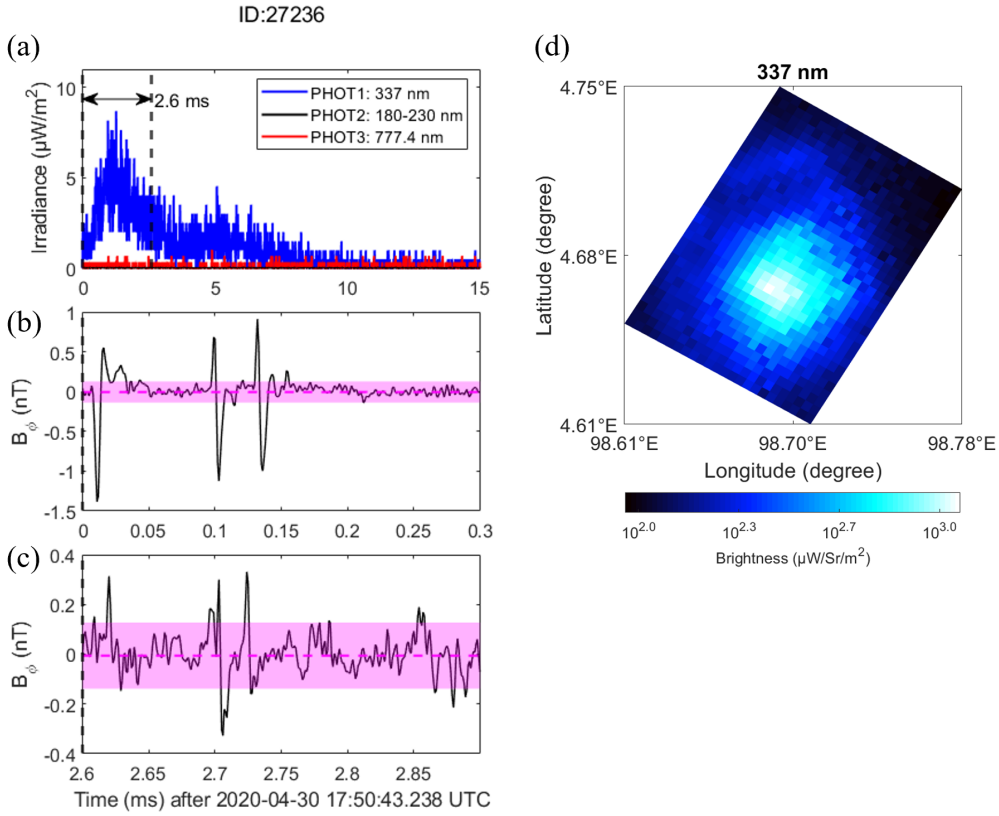

Figure S15. Comparison between MMIA photometer irradiance (blue: 337 nm, black: 180-230 nm and red: 777.4 nm) (a) and its corresponding NBE pulse (b) and the subsequent pulses trains (c) detected from the ground-based VLF/LF sensor nearby Malaysia for the multiple-pulse BLUE with ID 27236. The corresponding 337-nm filtered image of MMIA is shown in (d). Note that the subsequent pulse trains in (c) seems like a negative NBE, however, it is too noisy to identify it through the radio signals. The corresponding 337-nm filtered image of MMIA is shown in (d). The pink horizontal dashed line is the mean of the background noises with the pink shaded band $\mu \pm 3\sigma$.

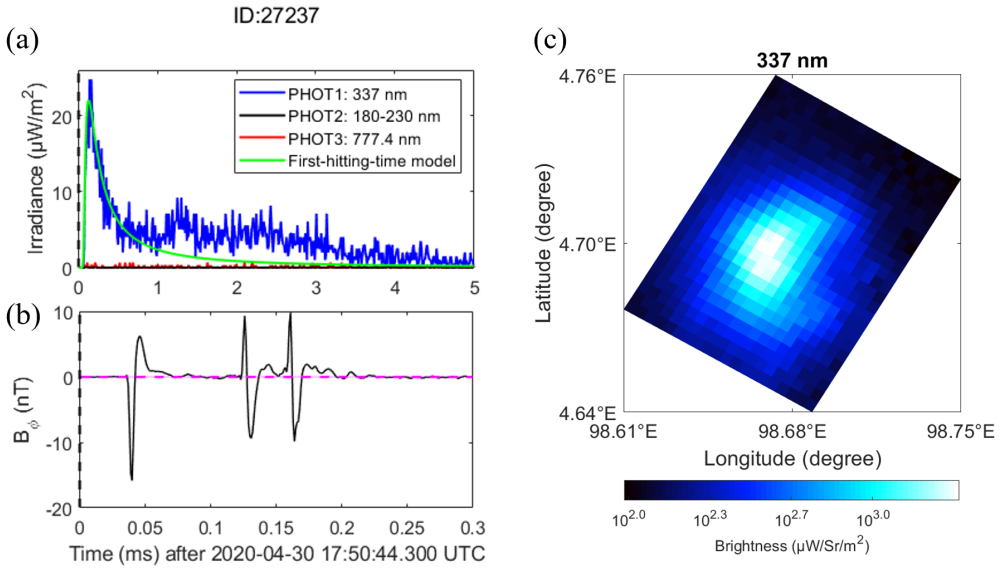

Figure S16. Comparison between MMIA photometer irradiance (blue: 337 nm, black: 180-230 nm, red: 777.4 nm and green: modeling result of the first-hitting-time model) (a) and its corresponding NBE pulse (b) detected from the ground-based VLF/LF sensor nearby Malaysia for the single-pulse BLUE with ID 27237. The corresponding 337-nm filtered image of MMIA is shown in (c). The pink horizontal dashed line is the mean of the background noises with the pink shaded band $\mu \pm 3\sigma$.

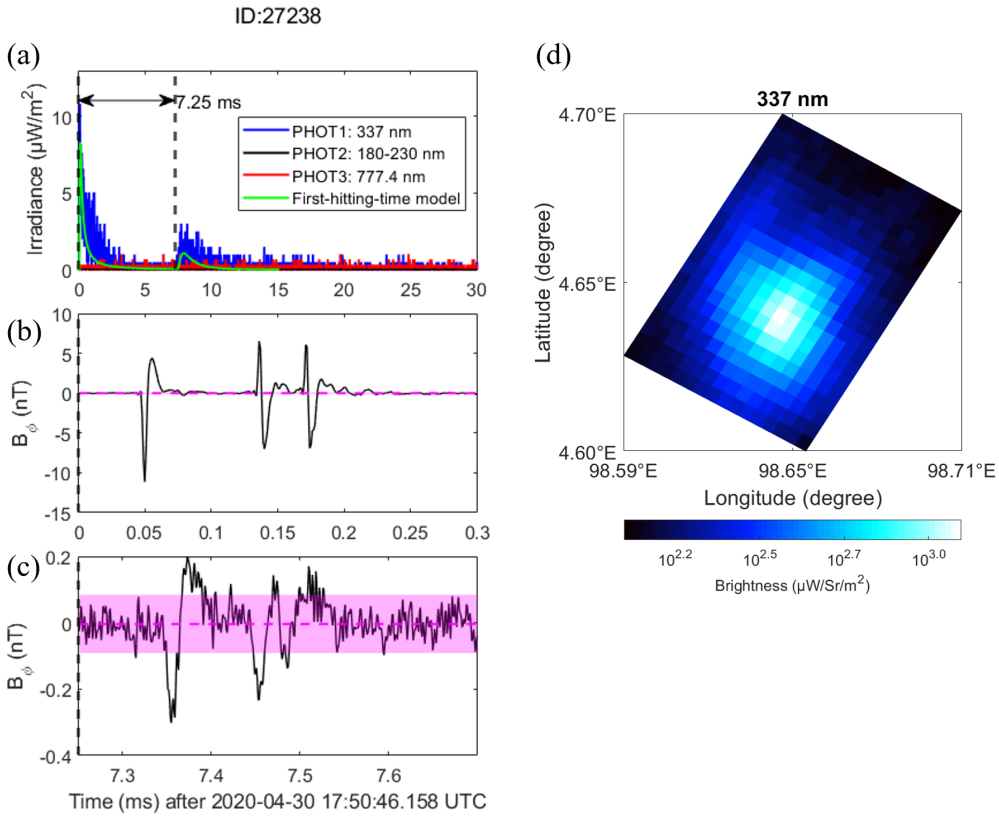

Figure S17. Comparison between MMIA photometer irradiance (blue: 337 nm, black: 180-230 nm, red: 777.4 nm and green: modeling result of the first-hitting-time model) (a) and its corresponding NBE pulse (b) and the subsequent pulses trains (c) detected from the ground-based VLF/LF sensor nearby Malaysia for the multiple-pulse BLUE with ID 27238. The corresponding 337-nm filtered image of MMIA is shown in (d). The subsequent pulse trains in (c) seems to be a "NBE-like" event, which might two NBE events occurred closely in time, however, it is too noisy to identify it through the radio signals. The pink horizontal dashed line is the mean of the background noises with the pink shaded band $\mu \pm 3\sigma$.

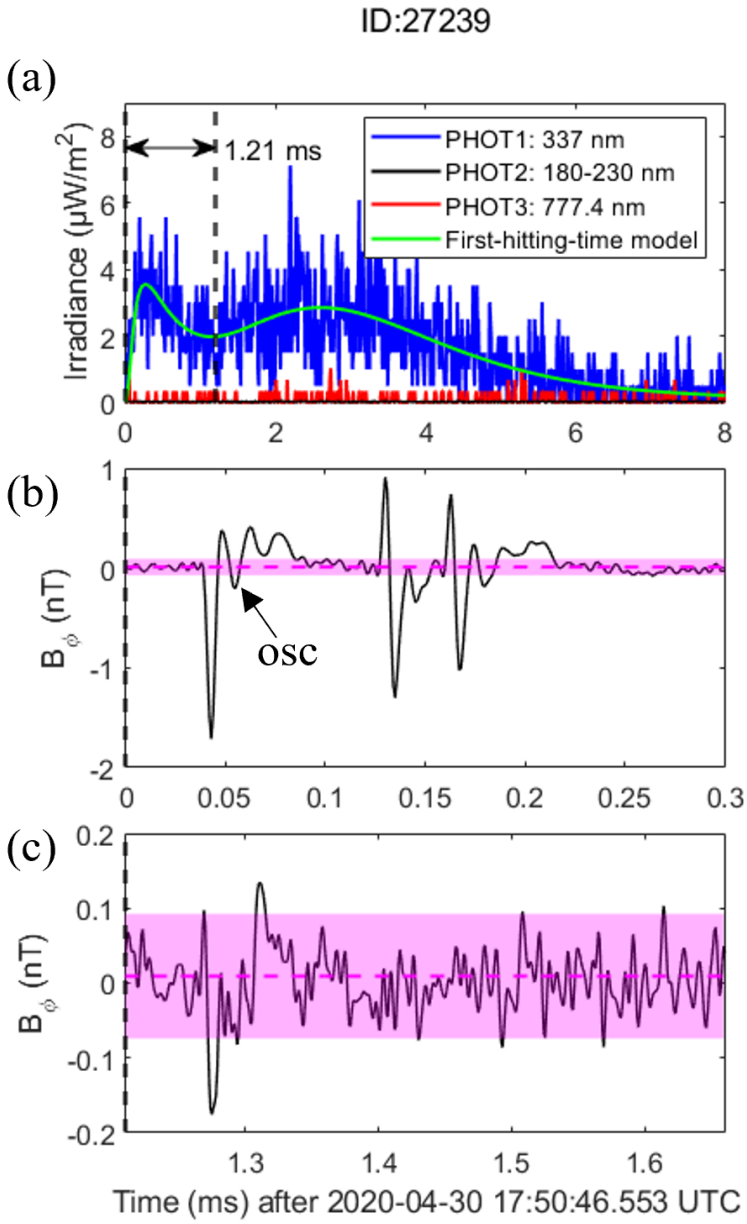

Figure S18. Comparison between MMIA photometer irradiance (blue: 337 nm, black: 180-230 nm, red: 777.4 nm and green: modeling result of the first-hitting-time model) (a) and its corresponding NBE pulse (b) and the subsequent pulses trains (c) detected from the ground-based VLF/LF sensor nearby Malaysia for the multiple-pulse BLUE with ID 27239. There is no corresponding 337-nm filtered image detected by MMIA. The pink horizontal dashed line is the mean of the background noises with the pink shaded band $\mu \pm 3\sigma$. The oscillations are marked as *OSC* in the figure.

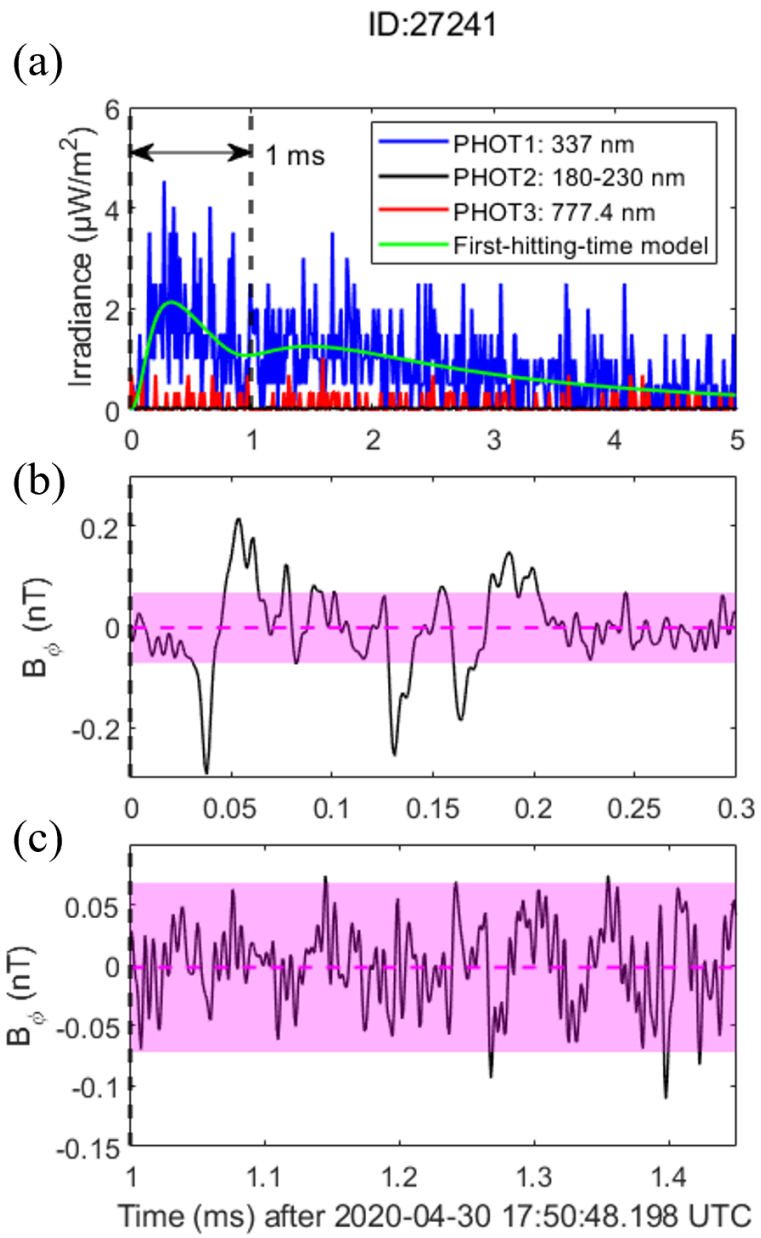

Figure S19. Comparison between MMIA photometer irradiance (blue: 337 nm, black: 180-230 nm, red: 777.4 nm and green: modeling result of the first-hitting-time model) (a) and its corresponding NBE pulse (b) and the subsequent pulses trains (c) detected from the ground-based VLF/LF sensor nearby Malaysia for the multiple-pulse BLUE with ID 27241. There is no corresponding 337-nm filtered image detected by MMIA. The pink horizontal dashed line is the mean of the background noises with the pink shaded band $\mu \pm 3\sigma$.

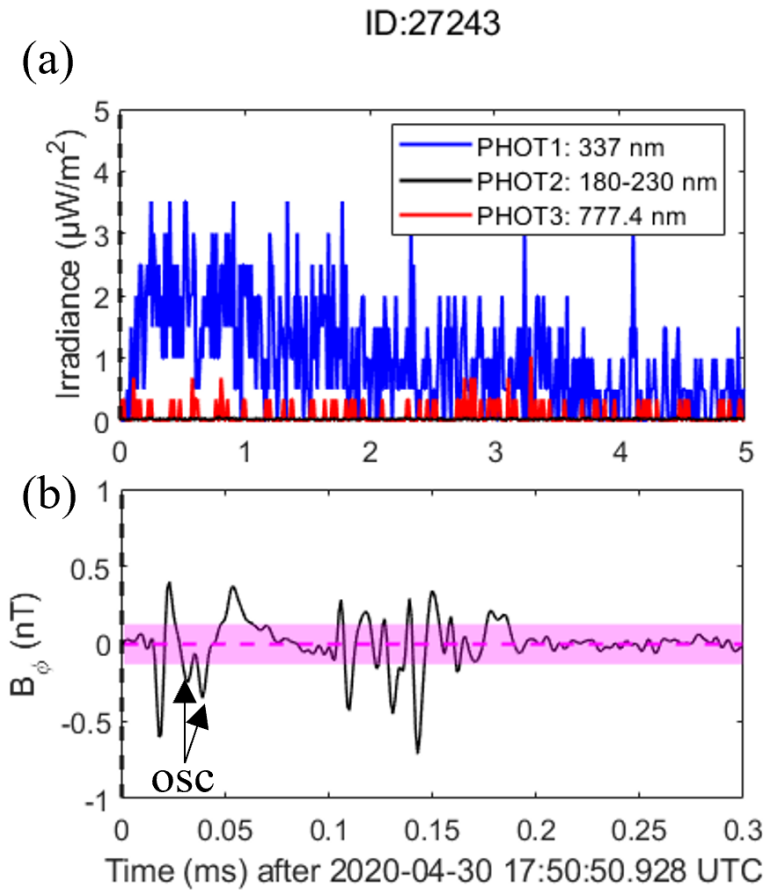

Figure S20. Comparison between MMIA photometer irradiance (blue: 337 nm, black: 180-230 nm and red: 777.4 nm) (a) and its corresponding NBE pulse (b) detected from the ground-based VLF/LF sensor nearby Malaysia for the single-pulse BLUE with ID 27243. There is no corresponding 337-nm filtered image detected by MMIA. The pink horizontal dashed line is the mean of the background noises with the pink shaded band $\mu \pm 3\sigma$. The oscillations are marked as *OSC* in the figure.

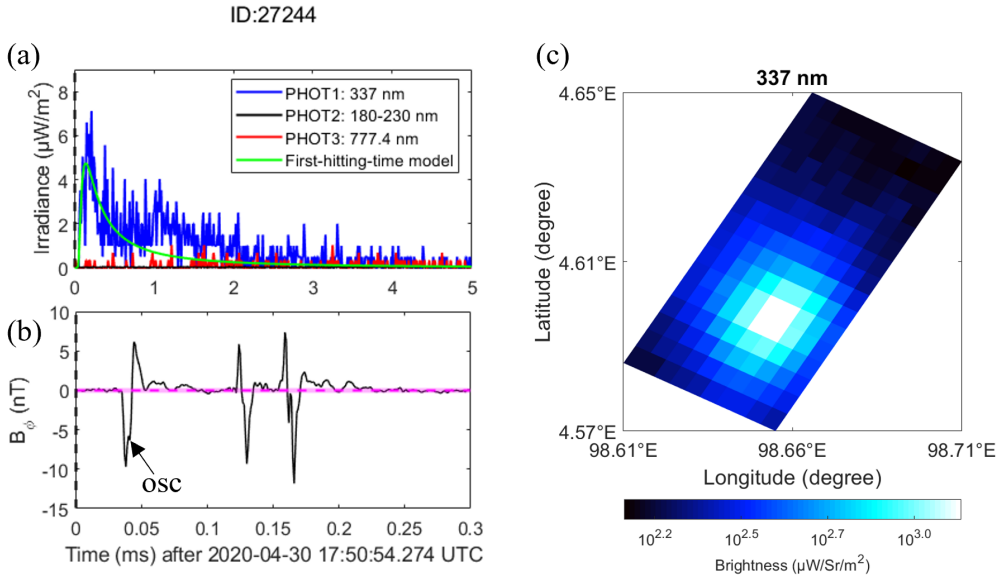

Figure S21. Comparison between MMIA photometer irradiance (blue: 337 nm, black: 180-230 nm, red: 777.4 nm and green: modeling result of the first-hitting-time model) (a) and its corresponding NBE pulse (b) detected from the ground-based VLF/LF sensor nearby Malaysia for the single-pulse BLUE with ID 27244. The corresponding 337-nm filtered image of MMIA is shown in (c). The pink horizontal dashed line is the mean of the background noises with the pink shaded band $\mu \pm 3\sigma$. The oscillations are marked as *OSC* in the figure.

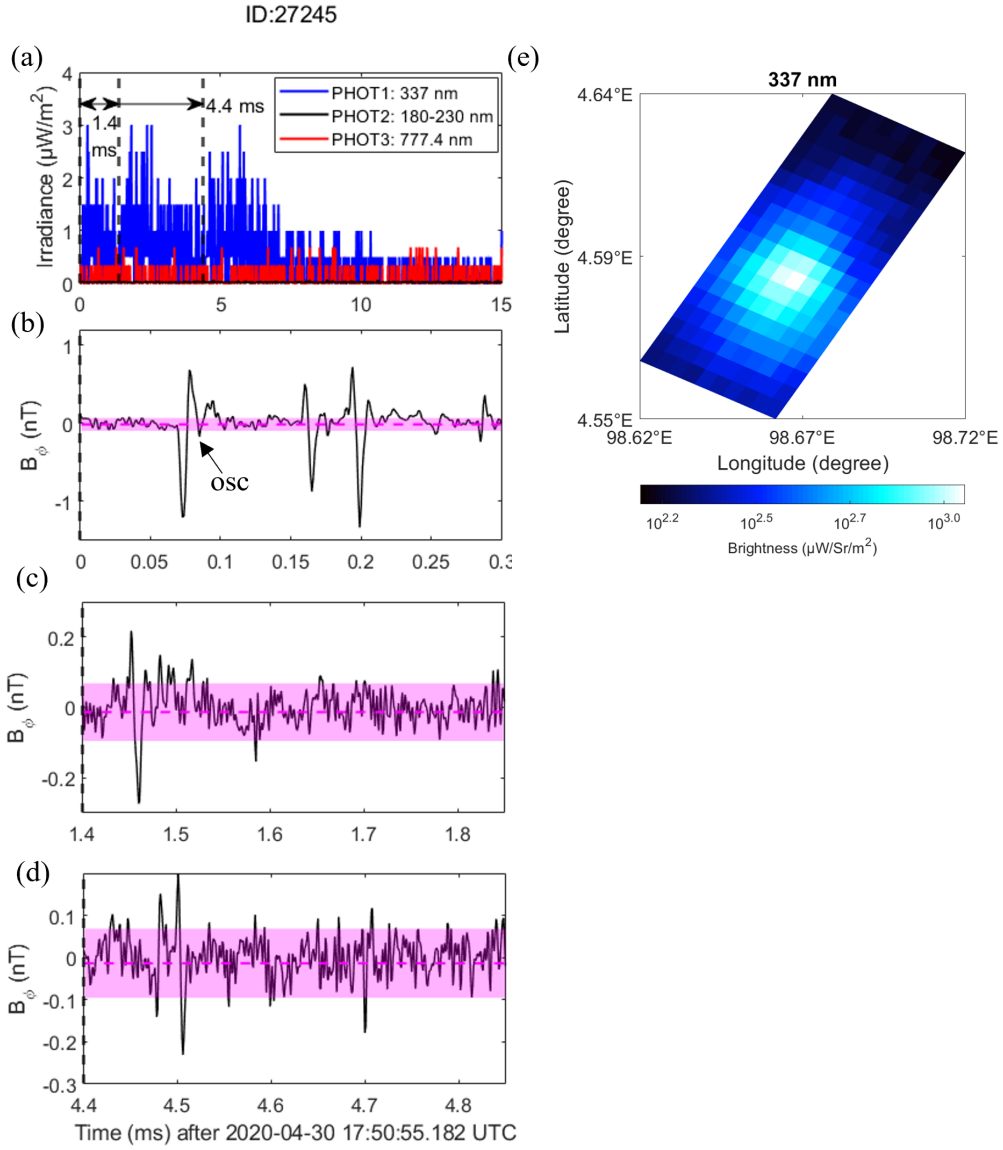

Figure S22. Comparison between MMIA photometer irradiance (blue: 337 nm, black: 180-230 nm and red: 777.4 nm) (a) and its corresponding NBE pulse (b), the first subsequent pulses trains after 1.4 ms (c) and the second subsequent pulses trains after 4.4 ms (d) detected from the ground-based VLF/LF sensor nearby Malaysia for the multiple-pulse BLUE with ID 27245. The corresponding 337-nm filtered image of MMIA is shown in (e). The pink horizontal dashed line is the mean of the background noises with the pink shaded band $\mu \pm 3\sigma$. The oscillations are marked as *OSC* in the figure.